Communications

A Patch Antenna With a Varactor-Loaded Slot for Reconfigurable Dual-Band Operation

Ahmed Khidre, Fan Yang, and Atef Z. Elsherbeni

***Abstract*—A new design approach for a microstrip patch antenna to achieve reconfigurable dual-band operation with tunable frequency ratio is introduced. The approach uses a lumped capacitor in the middle of a slotted patch antenna, which results in two resonant frequencies. The two resonant frequencies and their ratio are functions of the capacitance value. If a varactor with an appropriate biasing network is used, electronic tuning is realized by changing the applied DC voltage. To understand the dual-resonance behavior of the proposed antenna, an equivalent circuit model based on the transmission line theory of the antenna is established, considering the slot effect and the lumped capacitor. The results are verified with full wave simulation. Furthermore, measurements for fabricated antenna prototypes operating in 2–4.5 GHz are carried out for validation, and the performance shows a tunable frequency ratio from 1.45 to 1.93 with a capacitance range from 0.31 to 0.74 pF. It is worthwhile to point out that the radiation patterns are similar at both bands because both resonances are due to the fundamental TM01 mode.**

***Index Terms*—Circuit model, dual-band, frequency-agile, microstrip, patch, reconfigurable antennas, varactor diodes.**

I. Introduction

Dual-band antennas are of interest for wireless communication systems that use two bands of frequencies, such as Wi-Fi, and WiMax, because they could substitute for two individual antennas, which would reduce the implementation size, cost, and complexity. They provide also an advantage over wideband antennas, which is rejecting interference from coexisting services in the spectrum between the two operating bands. Many techniques have been reported for designing low cost, small profile, and efficient dual-band antennas as in [1]–[8]. Some techniques used a patch antenna at the higher order mode that has a quasi-similar radiation pattern of the fundamental mode [1]–[3]. Meanwhile, a slot antenna, which is another category of low cost small-profile antennas, is designed to provide dual-resonance in [4]–[6]. Other techniques for dual-band designs used parasitic elements in the proximity of the radiating element [7], multi-radiating elements [8], and stubs attached to the radiating elements [9]. These approaches are for fixed dual-band operation and do not allow for electronic tuning.

Frequency reconfigurable antennas are capable of changing their resonant frequency to operate at specific band along the multi-serviced radio spectrum. Therefore, they require less area for antenna terminals, and are more versatile for wireless devices. Such capability is also of interest for cognitive radio systems [10]. Significant advancements on frequency agile antennas were reported in the last few decades, such as in [11]–[18]. In [11]–[13], the patch antenna radiating edges are loaded with varactor diodes to allow for electronic tuning, whereas in [13] a PIN diode switch controls the length of the current path on the patch surface, producing frequency reconfigurability. Both methods have been employed together to a differential-fed patch antenna for a wider tuning range [14]. Similarly, frequency agile PIFA antennas have been also reported in [15], [16]. In addition to modifying the antenna aperture, a switchable/tunable matching circuit is used to reconfigure an antenna frequency band upon switching, or tuning its circuit components [17], [18].

Lately, some works have focused on the development of electronically tunable dual-band antenna designs. Tunable dual-band PIFA antennas are devised in [19]–[24], and the tuning mechanism is based on varactors or switches. In [25], [26], a varactor loaded-slot antenna is used at $\lambda/2$ and λ modes for the two resonant frequencies, which imposes some complications to obtain similar radiation patterns at both bands. Tunable dual-band antenna using PIFA and slot configurations are amenable for integration with hand-held devices due to their small sizes. However, they have smaller gain than their patch antenna counterpart that is more suitable for stationary terminals, base stations, and high gain antenna arrays.

In this communication, a new approach to design a fixed and reconfigurable dual-band microstrip patch antenna with tunable frequency ratio is introduced. The antenna geometry is a slotted patch with a capacitor loaded in the middle of the slot. The antenna dimensions and the capacitance value determine the two frequencies and their ratio. Consequently, tuning the frequency ratio is allowed by choosing the proper capacitor value. Moreover, if a varactor with an adequate biasing network is used instead, electronic tuning would be attained by changing the applied DC voltage. Because both resonant frequencies are due to the fundamental TM_{10} mode, similar radiation patterns are obtained at both bands. The transmission line theory along with the Wheeler incremental volume concept are utilized to build an equivalent circuit model that explains the dual-resonance behavior of the proposed antenna. The circuit model is validated with full wave simulations. Antenna prototypes operating within 2–4.5 GHz have been fabricated and measured, and the results show good agreement with the full wave simulations.

II. Dual-Band Antenna Design and Analysis

A. Antenna Geometry and Resonance Mechanism

The geometry of the proposed antenna design, labeled with dimensions, is shown in Fig. 1. It is a probe-fed patch antenna with a narrow rectangular slot carved on the center of the patch surface. The substrate is Rogers RT/duroid 5880 of permittivity $\varepsilon_r = 2.2$, thickness $h = 3.175$ mm, and loss tangent $\tan\delta = 0.0009$. The slot is loaded with a lumped capacitor of value C on its middle to control the current path length on the patch surface. Hence, continuous frequency tuning

Manuscript received October 07, 2013; revised October 06, 2014; accepted November 03, 2014. Date of publication December 02, 2014; date of current version January 30, 2015. This work was supported by the NASA EPSCoR program under Contract no. NNX09AP18A.

A. Khidre is with the Center of Applied Electromagnetic Systems Research (CAESR), Department of Electrical Engineering, The University of Mississippi, University, MS 38677 USA (e-mail: ahmed.khidre@ieee.org).

F. Yang is with the Center of Applied Electromagnetic Systems Research (CAESR), Department of Electrical Engineering, The University of Mississippi, University, MS 38677 USA and also with the Microwave and Antenna Institute, Department of Electronic Engineering, Tsinghua University, Beijing 100084, China (e-mail: fyang@olemiss.edu; fan_yang@tsinghua.edu.cn).

A. Z. Elsherbeni is with the Electrical Engineering and Computer Science Department, Colorado School of Mines, Golden, CO 80401 USA (e-mail: aelsherb@mines.edu).

Color versions of one or more of the figures in this communication are available online at http://ieeexplore.ieee.org.

Digital Object Identifier 10.1109/TAP.2014.2376524

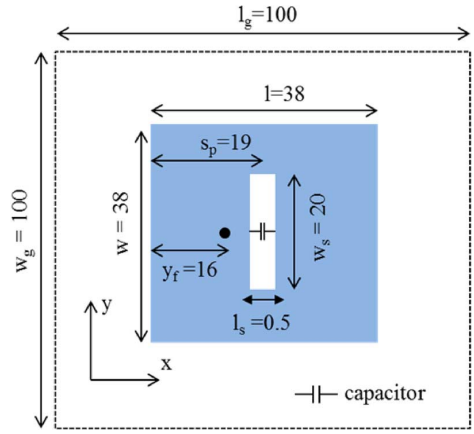

Fig. 1. Proposed patch antenna geometry with a slot centered on the patch and loaded with a capacitor in the middle. (units: mm).

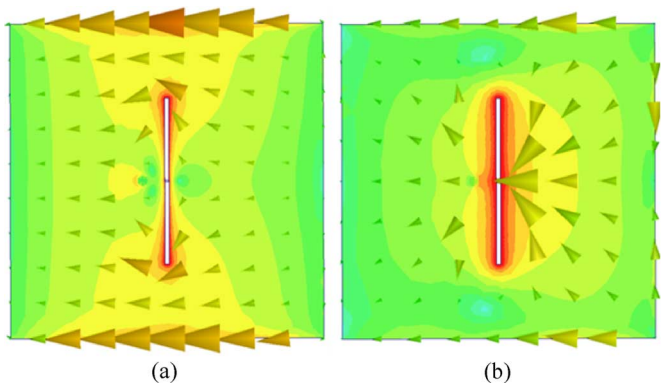

Fig. 2. Simulated current distributions of the proposed antenna with $C = 0.5$ pF at two resonant frequencies: (a) $f_1 = 2.275$ GHz; (b)$f_2 = 3.95$ GHz.

is then expected according to [13] through the change of the capacitance value C.

In contrast to [13], full wave simulations reveal that a dual-resonance behavior occurs when a proper capacitor is used. For instance, at $C = 0.5$ pF, two resonant frequencies $f_1 = 2.275$ GHz and $f_2 = 3.95$ GHz are observed. The original resonant frequency of the patch without the slot and capacitor is $f_0 = 2.45$ GHz. The full wave simulations on the proposed antenna are carried out using Ansoft HFSS [27]. The current distribution at each frequency has been inspected and plotted in Fig. 2. From the figure, it is observed that at the lower frequency, the current distribution is similar to the one of a plain patch but it detours around the slot, where the current path becomes longer. This explains why the first frequency f_1 is lower than the original resonant frequency $f_o (f_1 < f_o)$. At the higher frequency, the currents pass through the capacitor in the middle of the slot. Thus the lumped capacitor is equivalently seen in series with the antenna capacitance, reducing its overall value, and hence the second frequency is higher than the original resonant frequency $(f_2 > f_o)$. Because the current distribution of the second frequency has one maximum, it is still operating at the fundamental mode.

B. Equivalent Circuit Model

To better understand the dual-resonance mechanism of the proposed antenna, an equivalent circuit model is built using the transmission line theory, as shown in Fig. 3. A parallel connection of a resistor R_e and a capacitor C_e accounts for radiation and fringing fields at the patch edges $(x = 0, x = l)$. They are calculated from the formulas given in

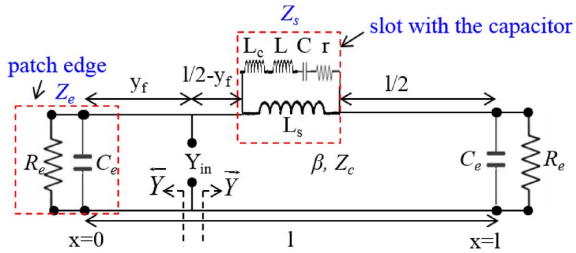

Fig. 3. Transmission line model of a patch antenna of length l with a capacitor-loaded slot.

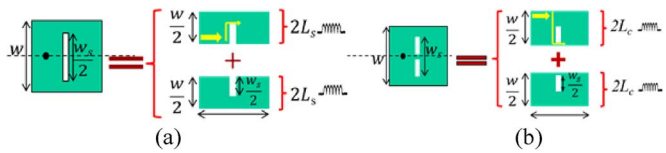

Fig. 4. A schematic diagram to illustrate how the wheeler volume concept is applied to calculate (a) the slot inductance (L_s), and (b) the series inductance to the capacitor (L_c).

[28]. The parameters β (propagation constant) and Z_c (characteristic impedance) are evaluated using the quasi-static formulas provided in [29]. The slot with the capacitor is modeled by a reactance Z_s, where C is the value of the capacitor placed in the middle of the slot, the series resistor r represents the inherent losses of the capacitor, and the series inductor L accounts for the package parasitic inductance. The values for r, and L could be obtained from the manufacturer data sheet or through measurements of the component. An additional inductance L_c is added serially to the capacitor to account for the effect of the current crowded through the capacitor. The parallel L_s represents the inductance accompanied by the current detour around the slot [30].

If the patch is seen as two halves, each is a microstrip line of width $w/2$, and intercepted by a narrow slit of width $w_s/2$ as shown in Fig. 4(a). Therefore, the inductance L_s due to the current going around the narrow slit could be calculated using equation (1), (2) deduced from the Wheeler incremental volume concept introduced in [31]. Z_W and Z_{W-Ws} in (2) are the air characteristic impedances for microstrip lines of widths W and $W - W_S$ respectively. Meanwhile, L_c is the inductance due the current path going through the capacitor along the whole microstrip line width $w/2$ as shown in Fig. 4(b). Therefore, using same concept, δ' in equation (1) approaches 0, and (3) is deduced to calculate L_c. The resonant frequency f_r as a function of C is evaluated by applying the resonance condition (4)

$$L_s = \frac{h\pi\mu_o}{4}\left(\frac{w' - \delta'}{w'}\right)^2 \tag{1}$$

$$w' = \frac{h}{Z_W}\sqrt{\frac{\mu_o}{\varepsilon_o}}, \quad \delta' = \frac{h}{Z_{W-Ws}}\sqrt{\frac{\mu_o}{\varepsilon_o}} \tag{2}$$

$$L_c = \frac{h\pi\mu_o}{4} \tag{3}$$

$$\mathrm{Im}\{Y_{in}(f_r, C)\} = \mathrm{Im}\left\{\overleftarrow{Y} + \overrightarrow{Y}\right\} = 0. \tag{4}$$

The numerical solution of (4) is plotted in Fig. 5, where it is compared with the full wave HFSS simulation results. Good correlation is observed between the circuit model results and HFSS results. Some deviations exist due the approximations in the empirical and quasi-static formulas used in the circuit model. Nevertheless, the circuit model gives a clear insight and understanding for the dual-resonance mechanism of the proposed design. Basically, the reactance Zs that models

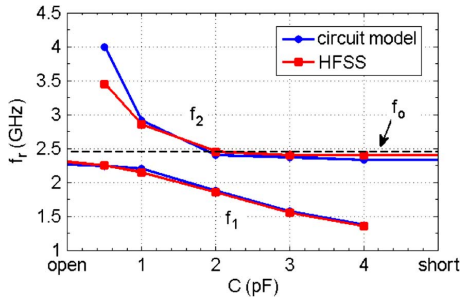

Fig. 5. Resonant frequencies of the proposed design versus the lumped capacitance value C.

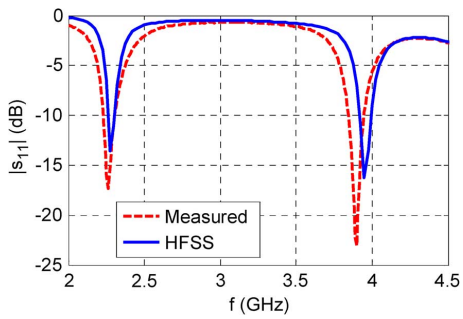

Fig. 6. Simulated and measured results for the power reflection coefficient of a dual-band patch antenna with a capacitor-loaded slot.

the slot with the capacitor is a resonant circuit, which is inductive at low frequency, and capacitive at high frequency. Hence, at certain capacitance value C, there exist two solutions for (4) that satisfy the resonance condition at the fundamental mode. The circuit model analysis is consistent with the qualitative explanation discussed in Section II-A. It is also observed that, at the open circuit condition ($C = 0$ pF), the antenna has single resonant frequency ($f_r = 2.25$ GHz) lower than the original f_o, whereas at the short circuit condition ($C = \infty$ pF) the resonant frequency ($f_r = 2.4$ GHz) gets closer to the f_o as concluded in [13].

The curve in Fig. 5 could be divided into three regions:

- Region 1, where $0 < C < 1$ pF: f_1 is relatively constant but f_2 varies significantly with C.
- Region 2, where $1 \leq C \leq 2$pF: both frequencies are dependent on C.
- Region 3, where $2 < C < \infty$ pF: f_1 changes with C but f_2 is almost constant.

It is also observed that the frequency ratio can go higher than 1.7, which is a quite high value for a dual-band antenna design using the fundamental mode of a single resonator. The reason for such a high ratio is the more pronounced change in the current path length with this new configuration compared to the one in [11], [12].

C. Antenna Performance

To demonstrate the radiation characteristics of the proposed antenna, the antenna in Fig. 1 has been fabricated and a surface-mount capacitor of 0.5 pF is used. The reflection coefficient is shown in Fig. 6. Good agreement is observed between the simulated and measured results. A slight downward frequency shift is observed in the measured results, and it is more noticeable at the higher band than the lower one. The larger tolerance in the capacitance value at the higher frequency is considered to be the main reason for this noticeable shift.

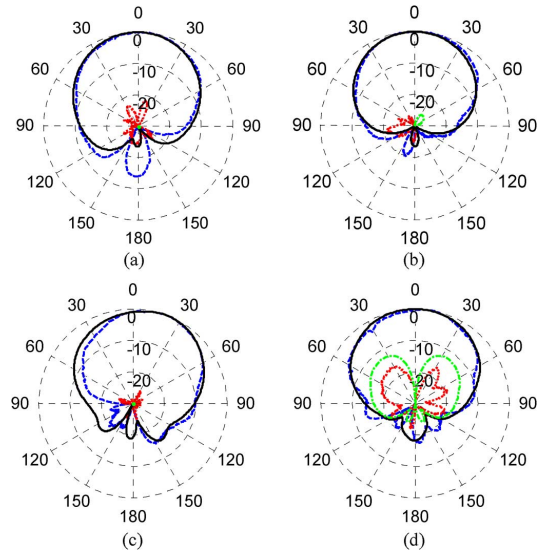

Fig. 7. Simulated co-pol radiation pattern (solid), simulated x-pol radiation patterns (dashed-dotted), measured co-pol radiation pattern (dashed), and measured x-pol radiation pattern (dotted) results in the principle cuts at both bands: (a) E-plane (xz) at 2.26GHz; (b) H-plane (yz) at 2.268 GHz; (c) E-plane (xz) at 3.89 GHz; (d) H-plane (xz) at 3.898 GHz.

The antenna radiation patterns at both bands in the E-plane (xz) and H-plane (yz) are presented in Fig. 7. Good agreement is observed between the simulated and measured results. The maximum measured x-pol level is -16.7 dB that occurs at the higher band. The measured realized gain at the lower and higher band is 7 dBi, and 5 dBi, respectively. The reduced gain at the higher band is thought to be due to the, higher I^2R loss in the lumped capacitor suffered by the patch current. Since, it has been previously shown in Fig. 2(b) that a large current is passing through the lumped capacitor at the higher band. It should be pointed out that the antenna operation in regions 2 and 3 ($1 < C < \infty$) is not suggested, in order to attain higher gain at f_2, because the capacitor loss is proportional to its capacitance value. It was also found that matching the antenna to 50 Ω is much easier in region 1 than in region 2 and 3 without the need of an additional matching circuit.

III. Reconfigurable Dual-Band Design

In the previous design, a fixed dual-band microstrip patch antenna has been achieved with the newly proposed antenna configuration in Fig. 1. One of the significant virtues of this new approach is the feasibility of electronic tuning by replacing the capacitor with a varactor diode plus a proper DC biasing circuit. Accordingly, a modification on the geometry in Fig. 1 has been done as shown in Fig. 8. A high quality varactor (SMV 1430) from Skyworks is used. It has a tuning range of $0.31 \leq \mathrm{C} \leq 1.24$ pF with $30 \leq \mathrm{V_{dc}} \leq 0V$, as shown in [32]. It is picked to cover Region 1 of the curve in Fig. 5. Region 1 is selected to avoid the gain drop at the higher band as discussed in Section II-C.

To build the DC biasing circuit, the patch is divided into two parts by a narrow slit, in order to avoid the DC short across the varactor diode terminals. Four low-loss surface-mount 68 nF capacitors are placed on the slit to maintain the RF continuity. The DC control signal will be supplied through the probe feed with a bias Tee that superimposes both RF and DC signals with high isolation (30 dB). For the completion of the DC path, the right part of the patch is grounded through a shorted transmission line with a metallic via. The transmission line is a stub using a radial sector at $\lambda_g/4$ (referred to 3 GHz) from the patch edge to form high impedance at that edge (RF choke). The dimensions of the transmission line and the radial stub were carefully designed to serve as

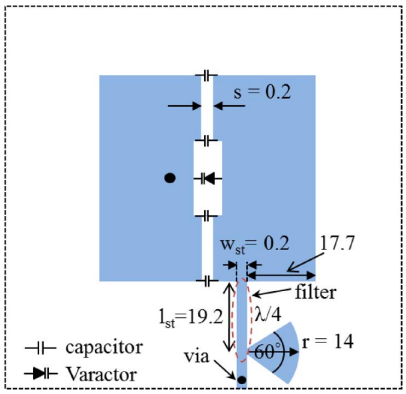

Fig. 8. Antenna geometry of a reconfigurable dual-band patch antenna with an integrated DC biasing network. (units: mm).

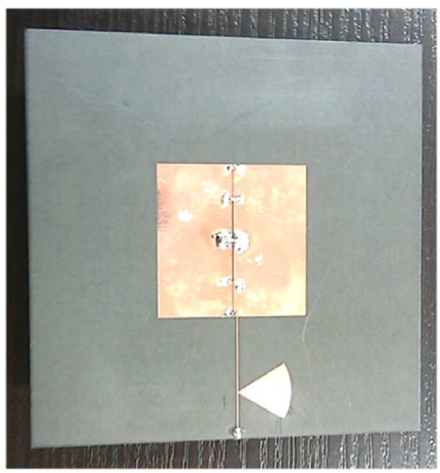

Fig. 9. Photo for the proposed reconfigurable dual-band patch antenna.

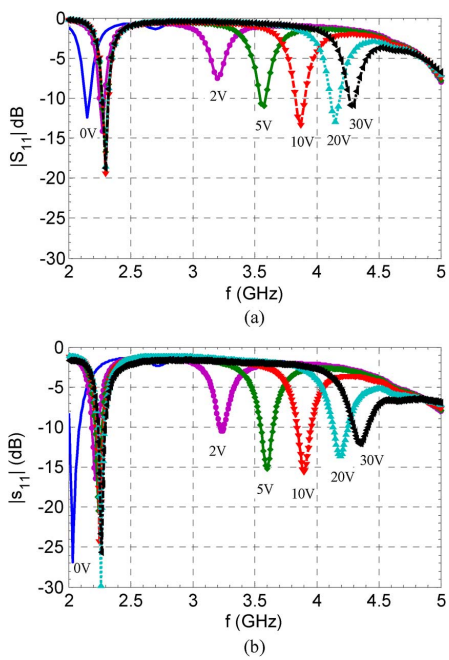

Fig. 10. The reflection coefficient of the proposed reconfigurable dual-band patch antenna versus the frequency at different DC biasing voltages: (a) simulation with HFSS; (b) measured with VNA.

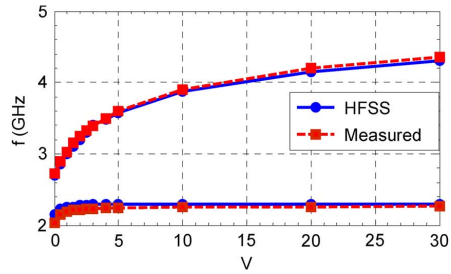

Fig. 11. The simulated and measured results for the first and second resonant frequencies of the proposed reconfigurable dual-band patch antenna versus the reverse DC biasing voltage.

a wideband stop filter with 20 dB isolation in the entire antenna operational band 2–4.5 GHz. A photo for the fabricated antenna prototype is shown in Fig. 9.

The antenna reflection coefficient at different DC voltages is shown in Fig. 10. Good agreement between the simulated and measured results is observed. As expected, by changing the biasing voltage from 0 to 30 volts that corresponds to changing the capacitance C from 2.24 to 0.31 pF, the second resonance f_2 is being tuned, whereas the first resonance f_1 is relatively constant (operation in region 1). The simulated reflection coefficient at different DC voltages is obtained by matching the diode reverse voltage with its associated capacitance, as determined from the $C-V$ curve in [32]. From Fig. 10(b), it is clear that the useful tuning range is from 2 to 30 volts, where the antenna is well matched $(S^{11} \leq -10\ \text{dB})$.

The resonant frequencies versus the reverse bias voltages are plotted in Fig. 11. A small deviation is observed between the simulated and measured results. This is attributed to the minor deviation of the capacitance value C from the $C-V$ curve in [32], which is given at low frequency (<500 MHz). Along the useful tuning range $2 \leq \text{V}_{\text{dc}} \leq 30$, the measured f_1 changes from 2.22 to 2.26 GHz, whereas the measured f_2 changes from 3.24 to 4.35 GHz. The measured ratio (f_2/f_1) between the two resonant frequencies changes from 1.45 to 1.93, which is a significantly large tuning ratio with $2 \leq \text{V}_{\text{dc}} \leq 30$ V that corresponds to $0.74 > C > 0.31$ pF.

The antenna radiation patterns in the principle planes at different applied DC biasing voltages have been measured and plotted in Fig. 12. The co-pol patterns are similar at both bands because radiations at both bands are due to the fundamental TM_{01} mode. The cross polarized level within the 3 dB beam width is < -18 dB for the lower band, whereas for the higher band it is -10.6 dB at most. Pattern stability along different voltages at both bands is observed. The realized gain at both bands is measured along the entire tuning range (2–30 volts), and the results are shown in Fig. 13. The average gain at the lower band is 7 dBi, whereas at the higher band, the gain varies from 4 to 6.8 dBi. The difference between measured and simulated results is due to the ambiguous losses introduced by the varactor along with its associated biasing circuit. The antenna efficiency at both bands is measured, and its value across the tuning range is almost 89% at the lower band, and varies from 38% to 90% at the higher band. The gain and efficiency are almost constant with the biasing voltage for the lower band because f_1 is almost constant. However, for the higher band as the voltage increases (capacitance decreases) the efficiency and the gain increase. The efficiency and consequently the gain enhancement with the voltage growth are because the varactor loss decreases as the voltage increases, which agrees with the proportionate relation between the varactor loss and its capacitance value [14]. Another reason that contributes to the gain enhancement with the voltage growth is the increase of the second resonant frequency f_2 and hence, for fixed physical size, the antenna

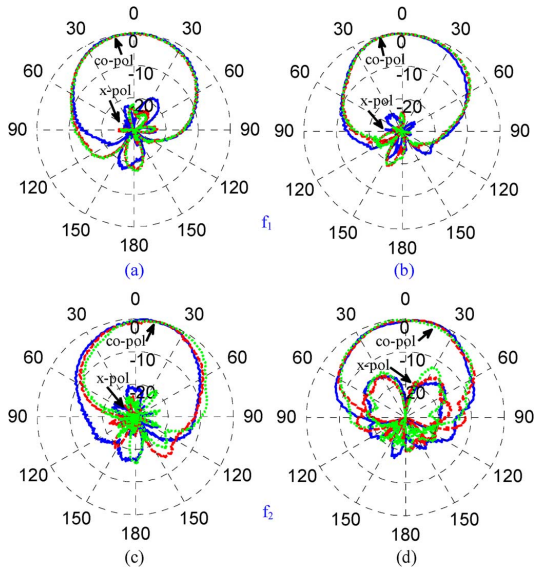

Fig. 12. The measured results in the lower and higher bands for the co-pol, and x-pol radiation patterns in the principle planes at 2v (solid), 10v (dashed), and 20v (dotted): (a) xz plane (e-plane) in lower band; (b) yz plane (h-plane) in lower band; (c) xz plane (e-plane) in higher band; (d) yz plane (h-plane) in higher band.

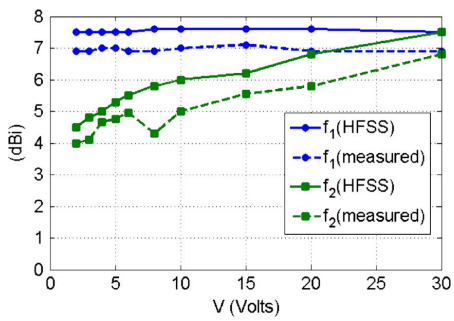

Fig. 13. The simulated and measured gain of the proposed reconfigurable dual-band patch antenna at both bands versus the reverse DC biasing voltage (the corresponding frequencies are shown in Fig. 11).

electrical size becomes larger. This enlargement of the antenna's electrical size (aperture) enhances its gain as described in [33]. Regarding the higher band, better antenna efficiency could be attained if a higher quality varactor is used. Newly emerged technologies are needed to enable high-quality varactors for high frequency applications.

IV. Conclusion

A novel approach for the design of a dual-band microstrip patch antenna using a capacitor-loaded slot has been proposed in this communication. The capacitor-loaded slot is inductive at a band of lower frequencies and capacitive at a band of higher frequencies, leading to a dual resonance mechanism (two solutions for the resonance conditions) of the microstrip patch. The proposed technique also shows the feasibility of an electronically reconfigurable dual-band operation whose tuning mechanism relies on a varactor diode. The frequency ratio is tuned from 1.45 to 1.93 with 0.31- 0.74 pF capacitance range, and 2–30 volts DC voltage. Similar radiation patterns at both bands are obtained because of the same resonant mode. The realized gain at the lower band (from 2.22 to 2.26 GHz) is 7 dBi with 89% efficiency; whereas at the higher band (from 3.24 to 4.35 GHz) it changes from 4 to 6.8 dBi with the corresponding efficiency varies from 38% to 90%. Better efficiency could be obtained with advanced enabling technologies for fixed or variable capacitors that allow for higher quality factors. The attained gain values are higher than the current designs of tunable dual-band PIFA and slot antennas, making it a good candidate for the base stations and terminals of wireless networks, including cognitive and software defined radio systems.

Acknowledgment

The authors would like to acknowledge Rogers Corporation for supplying microwave dielectric substrates used for the fabrication of the antenna prototypes.

References

[1] S. Maci, B. B. Gentili, P. Piazzesi, and C. Salvador, "Dual band slot-loaded patch antenna," *IEEE Antennas Propag. Mag.*, vol. 39, no. 6, pp. 13–20, Dec. 1997.

[2] K. B. Hsieh and K. Wong, "Inset microstrip-line-fed dual-frequency circular microstrip antenna and its application to a two-element dual-frequency microstrip array," in *Inst. Elect. Eng. Microw. Antennas Propag. Symp. Digest*, Oct. 1999, vol. 147, pp. 359–361.

[3] S. T. Fang and K. L. Wong, "A dual frequency equilateral triangular microstrip antenna with a pair of two narrow slots," *Microw. Opt. Technol. Lett.*, vol. 23, pp. 82–84, Oct. 1999.

[4] D. Llorens, P. Otero, and C. C. Penalosa, "Dual-band, single CPW port, planar slot antenna," in *IEEE Int. Antennas and Propagation Symp. Digest*, 2003, pp. 137–139.

[5] C. Wang, J. Lee, and R. Huang, "Experimental studies of a miniaturized CPW-fed slot antenna with the dual-frequency operation," *IEEE Antennas Wireless Propag. Lett.*, vol. 2, pp. 151–154, 2003.

[6] T. Morioka, S. Araki, and K. Hirasawa, "Slot antenna with parasitic element for dual band operation," *IET Electron. Lett.*, vol. 33, pp. 2093–20944, Dec. 1997.

[7] K. Virga and Y. Rahmat-Samii, "Low-profile enhanced-bandwidth PIFA antennas for wireless communications packaging," *IEEE Trans. Microw. Theory Techn.*, vol. 45, no. 10, pp. 1879–1888, Oct. 1997.

[8] K. L. Wong, *Compact and Broadband Microstrip Antennas*. New York, NY, USA: Wiley, 2002.

[9] K. P. Ray and G. Kumar, "Tunable and dual-band circular microstrip antenna with stubs.," *IEEE Trans. Antennas Propag.*, vol. 48, no. 7, July 2000.

[10] Y. Tawk, J. Costantine, K. Avery, and C. G. Christodoulou, "Implementation of a cognitive radio front-end using rotatable controlled reconfigurable antennas," *IEEE Trans. Antennas Propag.*, vol. 59, no. 5, pp. 1773–1778, May 2011.

[11] D. Schaubert, F. Farrar, A. Sindoris, and S. Hayes, "Microstrip antennas with frequency agility and polarization diversity," *IEEE Trans. Antennas Propag.*, vol. 29, no. 1, pp. 118–123, Jan. 1981.

[12] P. Bhartia and I. J. Bahl, "Frequency agile microstrip antennas," *Microw. J.*, pp. 67–70, Oct. 1982.

[13] F. Yang and Y. Rahamt-Samii, "Patch antennas with switchable slots (PASS) in wireless communications: Concepts, designs, applications," *IEEE Antennas Propag. Mag.*, vol. 47, no. 2, pp. 13–29, April 2005.

[14] S. Hum and H. Xiong, "Analysis and design of a differentially-fed frequency agile microstrip patch antenna," *IEEE Trans. Antennas Propag.*, vol. 58, no. 10, pp. 3122–3130, Oct. 2010.

[15] P. Panayi, M. Al-Nuaimi, and I. Ivrissimtzis, "Tuning techniques for planar inverted-F antenna," *Electron. Lett.*, vol. 37, no. 16, pp. 1003–1004, Aug. 2001.

[16] A. Sheta and S. Mahmoud, "A widely tunable compact patch antenna," *IEEE Antennas Wireless Propag. Lett.*, vol. 7, pp. 40–42, 2008.

[17] Y. Li, Z. Zhang, W. Chen, and Z. Feng, "A switchable matching circuit for compact wideband antenna designs," *IEEE Trans. Antennas Propag.*, vol. 58, no. 11, pp. 3450–3457, Nov. 2010.

[18] Y. Li, Z. Zhang, W. Chen, Z. Feng, and M. Iskander, "A compact DVB-H antenna with varactor-tuned matching circuit," *Microw. Opt. Technol. Lett.*, vol. 52, no. 8, pp. 1786–1789, Aug. 2010.

[19] V. A. Nguyen, R. A. Bhatti, and S. O. Park, "A simple PIFA-based tunable internal antenna for personal communication handsets," *IEEE Antennas Wireless Propag. Lett.*, vol. 7, pp. 130–133, 2008.

[20] A. Sheta and M. Alkanhal, "Compact dual-band tunable microstrip antenna for Gsm/DCS-1800 applications," *IET Proc. Microw. Antennas Propag.*, vol. 2, no. 3, pp. 274–280, Apr. 2008.

[21] S.-K. Oh, H.-S. Yoon, and S.-O. Park, "A PIFA-type varactor-tunable slim antenna with A PIL patch feed for multiband applications," *IEEE Antennas Wireless Propag. Lett.*, vol. 6, pp. 103–105, 2007.

[22] N. Karmakar, "Shorting strap tunable stacked patch PIFA," *IEEE Trans. Antennas Propag.*, vol. 52, no. 11, pp. 2877–2884, Nov. 2004.

[23] A. Mak, C. Rowell, R. Murch, and C. Mak, "Reconfigurable multiband antenna designs for wireless communication devices," *IEEE Trans. Antennas Propag.*, vol. 55, no. 7, pp. 1919–1928, Jul. 2007.
[24] M. Komulainen, M. Berg, H. Jantunen, E. Salonen, and C. Free, "A frequency tuning method for a planar inverted-F antenna," *IEEE Trans. Antennas Propag.*, vol. 56, no. 4, pp. 944–950, Apr. 2008.
[25] N. Behdad and K. Sarabandi, "A varactor tuned dual-band slot antenna," *IEEE Trans. Antennas Propag.*, vol. 54, no. 2, pp. 401–408, Feb. 2006.
[26] N. Behdad and K. Sarabandi, "Dual-band reconfigurable antenna with a very wide tunable range," *IEEE Trans. Antennas Propag.*, vol. 54, no. 2, pp. 409–416, Feb. 2006.
[27] High Frequency Structure Simulation (HFSS) ver. 13, Ansoft Corp.. Canonsburg, PA, 2010.
[28] K. Carver and J. Mink, "Microstrip antenna technology," *IEEE Trans. Antennas Propag.*, vol. 29, no. 1, pp. 2–24, 1981.
[29] K. Gupta, R. Garg, I. Bahl, and P. Bhartia, *Microstrip Lines and Slotlines*, 2nd ed. Boston, MA, USA: Artech House, 1996.
[30] X. Zhang and F. Yang, "Study of a slit cut on a microstrip antenna and its applications," *Microw. Opt. Technol. Lett.*, vol. 18, no. 4, pp. 297–300, July 1998.
[31] W. Hoefer, "Equivalent series inductivity of a narrow transverse slit in microstrip," *IEEE Trans. Microw. Theory Techn.*, vol. 25, no. 10, pp. 822–824, Oct. 1977.
[32] Data Sheet of Skyworks Varactor Diodes SMV1405-SMV1430 Series: Plastic Packaged Abrupt Junction Tuning Varactors.
[33] L. J. Chu, "Physical limitations on omni-directional antennas," *J. Appl. Phys.*, vol. 19, pp. 1163–1175, Dec. 1948.

Study and Design of Broadband Bow-tie Slot Antenna Fed With Asymmetric CPW

Lina Xu, Li Li, and Wenmei Zhang

***Abstract*—In this communication, a new style of broadband bow-tie slot antenna with an improved gain is presented. It is fed by an asymmetric coplanar waveguide (ACPW) with different slot lengths. By adjusting the length of one ACPW slot, the impedance characteristic of the antenna is greatly improved so that the bandwidth is broadened. Meanwhile, to improve the gain at low frequency band, a loop strip is added in the bow-tie slot. The simulated and measured results show that the proposed antenna can operate from 2.76 GHz to 8.1 GHz and the relative bandwidth is 100.4%. Furthermore, the flatter gain within the operating frequency band is obtained and the maximum gain at beam peak reaches 5.53 dBi.**

***Index Terms*—Bow-tie slot, broadband, coplanar waveguide (CPW)-fed, flexible antenna.**

I. Introduction

With the rapid developments in wireless communication technology, higher requirements are put forward to antenna system. Wideband and compact antennas are required by global positioning system (GPS), satellite communications system, and personal communications system. Bow-tie slot antennas with wide bandwidth and compact structure have received widespread attention. Durgun *et al.* proposed an improved bow-tie antenna with reduced metallization based on the phenomenon that the majority of the current density was confined towards the edges of the patch. After the centers of the triangular parts were removed, the performance of antenna did not have significant variation [1]. Huang *et al.* studied the influence of slot width and the extended angle on the CPW-fed bow-tie slot antenna. By changing the slot width, a 36% bandwidth ($\mathrm{VSWR} < 2$) was obtained when the extended angle was 20° [2]. Soliman *et al.* studied the performance of the CPW-fed bow-tie slot antenna with different flare angles of the bow-tie slot. The results showed that a higher bandwidth of 34.6% was achieved when the flare angle is 90° [3]. Eldek *et al.* analyzed the influence of all the antenna parameters on the bandwidth of the CPW-fed bow-tie slot antenna, and proposed a bow-tie slot antenna with 40% bandwidth for radar applications [4]. Niu *et al.* presented a broadband CPW-fed bow-tie slot antenna. By using a linear tapered transition to connect the bow-tie radiation slot and the gaps of the feed line, a 37% bandwidth was achieved [5]. Marantis *et al.* realized a CPW-fed bow-tie slot antenna with a 55% impedance bandwidth by introducing two metal stubs in the middle of the bow-tie slot [6]. Hou *et al.* presented a dual-band bow-tie slot antenna for WiFi and WiMAX system applications. The designed antenna utilized the coplanar waveguide (CPW) feeding with the inductive coupling. Its dual-band feature was constituted by the primary and secondary bow-tie slots with special feeding-slot arrangements [7].

In this communication, a new type of broadband and high-gain bow-tie slot antenna fed by an asymmetric CPW (ACPW) is presented. To achieve a wider impedance bandwidth, one of the CPW slots is lengthened and an ACPW with different lengths of slots are formed. Also, by introducing two loop strips in the bow-tie slots, the gain at low frequencies is increased. The measured results show that the proposed antenna has a bandwidth of 5.34 GHz (from 2.76 GHz to 8.1 GHz) and the relative bandwidth is 100.4%. Furthermore, the gain at beam peak over the entire operating range is better than 1.5 dBi and the maximum gain is 5.53 dBi.

II. Design of Broadband Bow-Tie Slot Antenna

The proposed broadband antenna is shown in Fig. 1. It consists of a ground plane on one side of a dielectric substrate. The white parts on the ground plane are slots and the gray part is the metal. The antenna is fed with a CPW. To improve the antenna bandwidth, a stub is introduced. As a result, one of the CPW slots is lengthened and an asymmetric CPW (ACPW) with different lengths of slots is formed. The antenna is realized on the Rogers RT/duroid 5880(tm) substrate with $\varepsilon_{\mathrm{r}} = 2.2$ and $h = 1.6$ mm. Its dimension is $53\ \mathrm{mm} \times 25.25\ \mathrm{mm}$. The dimensions of the antenna are shown in Table I.

First, the working mechanism of ACPW is investigated by analyzing surface current distribution. The magnitude and vector plot of surface current density at 3 GHz is illustrated in Fig. 2. It shows that the current in the center strip conductor mainly flows along the slot due to a larger S_{w}. In this case, the additional slot path gives rise to a cascaded capacitance C_{s}. The larger the l_3 is, the larger the capacitance C_{s} is. The increased C_{s} will cause the resonant frequency of antenna decrease. Also, the additional slot path introduces the phase delay in the two branches by adjusting l_3.

Manuscript received June 09, 2014; revised September 24, 2014; accepted November 25, 2014. Date of publication December 05, 2014; date of current version January 30, 2015. This work was supported in part by the National Science Foundation of China under Grants (61271160, 61172045, 61178013), the National Fundamental Fund of Personal Training under Grant (J1210036), the Shanxi Scholarship Council of China under Grant (2012-014), and in part by the Research Fund for the Doctoral Program of Higher Education under Grant (20121401110009).

The authors are with the College of Physics and Electronics, Shanxi University, Shanxi 030006, China (e-mail:zhangwm@sxu.edu.cn).

Color versions of one or more of the figures in this communication are available online at http://ieeexplore.ieee.org.

Digital Object Identifier 10.1109/TAP.2014.2378265